bioRxiv preprint doi: https://doi.org/10.1101/806885; this version posted October 17, 2019. The copyright holder for this preprint (which was not certified by peer review) is the author/funder. All rights reserved. No reuse allowed without permission.

Precise regulation of the relative rates of surface area and volume synthesis in dynamic environments

Handuo Shi[1], Yan Hu[1], Kerwyn Casey Huang[1,2,3,*]

[1]Department of Bioengineering, Stanford University, Stanford, CA 94305, USA

[2]Department of Microbiology and Immunology, Stanford University School of Medicine, Stanford, CA 94305, USA

[3]Chan Zuckerberg Biohub, San Francisco, CA 94158

[*]To whom correspondence should be addressed: kchuang@stanford.edu

Keywords: *Escherichia coli*, *Bacillus subtilis*, *Caulobacter crescentus*, *Schizosacccharomyces pombe*, cell-size control, surface area to volume ratio, cell morphology, cell elongation, cell division

bioRxiv preprint doi: https://doi.org/10.1101/806885; this version posted October 17, 2019. The copyright holder for this preprint (which was not certified by peer review) is the author/funder. All rights reserved. No reuse allowed without permission.

Abstract

Bacterial cells constantly face complex environmental changes in their natural habitats. While steady-state cell size correlates with nutrient-determined growth rate, it remains unclear how cells regulate their morphology during rapid environmental changes. Here, we systematically quantified cellular dimensions throughout passage cycles of stationary-phase cells diluted into fresh medium and grown back to saturation, and found that cells exhibit characteristic dynamics in surface area to volume ratio (SA/V). SA/V dynamics were conserved across many genetic/chemical perturbations, as well as across species and growth temperatures. We developed a model with a single fitting parameter, the time delay between surface and volume synthesis, that quantitatively explained our SA/V observations, and showed that the time delay was indeed due to differential expression of volume and surface-related genes. The first division after dilution occurred at a tightly controlled SA/V, a previously unrecognized size-control mechanism highlighting the relevance of SA/V. Finally, our time-delay model successfully predicted the quantitative changes in SA/V dynamics due to altered surface area synthesis rates or time delays from translation inhibition. Our minimal model thus provides insight into how cells regulate their morphologies through differential regulation of surface area and volume synthesis and potentiates deep understanding of the connections between growth rate and cell shape in complex environments.

bioRxiv preprint doi: https://doi.org/10.1101/806885; this version posted October 17, 2019. The copyright holder for this preprint (which was not certified by peer review) is the author/funder. All rights reserved. No reuse allowed without permission.

Introduction

In their natural habitats, bacterial cells constantly face dynamic environmental conditions. To survive, cells alter their physiology to cope with stresses such as nutrient depletion, chemical inhibition, and temperature shifts. During stressful conditions, cells alter their gene expression profiles, often slowing down growth and proliferation and instead allocating limited resources to genes critical for survival[1]. While certain genetic perturbations do not have observable effects in fast-growing cells, they cause death in stressed conditions[2] or impair survivability when cells resume growth after the environment becomes favorable again[3,4], highlighting the unique physiological challenges posed by dynamic environments.

Cell shape is intrinsically linked to physiology. During steady-state growth, fast-growing cells in nutrient-rich media adopt larger volumes compared to isogenic cells in minimal media[5], and systematic tuning of growth rate via medium composition dictates steady-state cell size[6]. Gene expression is also modulated by steady-state growth rates: faster-growing cells tend to have a higher fraction of their proteome devoted to ribosomes, addressing the need for rapid protein synthesis[7,8]. In a batch culture, cell shape can undergo transitions in both cell width and length within several minutes[9,10], in part as cells adapt their transcriptional program to the new medium and also because the growth of cells can alter the medium composition through nutrient depletion and

bioRxiv preprint doi: https://doi.org/10.1101/806885; this version posted October 17, 2019. The copyright holder for this preprint (which was not certified by peer review) is the author/funder. All rights reserved. No reuse allowed without permission.

waste production. Previously, a top-down flux-balance model accurately depicted the kinetics of gene expression and growth in *Escherichia coli* cells under nutrient shifts[11], but it remains unclear how these environmental and gene expression changes are transduced into cell-shape changes, and whether cell shape is actively optimized in a dynamic environment or is simply a passive outcome of cellular physiology.

In most bacteria, cell shape and size are dictated by the cell wall, a rigid network of peptidoglycan[12,13]. To grow and divide, cells synthesize new peptidoglycan precursors in the cytoplasm, which are then transported to the periplasm and inserted to the expanding cell wall[13]. In rod-shaped bacteria such as *Escherichia coli*, cell elongation and division are regulated by distinct machineries. The actin homolog MreB dictates the insertion pattern of new peptidoglycan material along the cylindrical cell body[14], which elongates the cell and maintains steady-state cell width[15]. Cell division is regulated by FtsZ, a tubulin homolog that localizes to the mid-cell and forms a ring-like structure prior to division, which then constricts and guides septum formation[13]. Chemical or genetic perturbations to the elongation or division machinery alter cell-shape homeostasis through modified patterns of cell wall synthesis[9,10,15-18]. The extent to which such perturbations disrupt the ability of bacterial cells to adjust to new environments could provide insight into the cellular processes key to shape adaptation.

bioRxiv preprint doi: https://doi.org/10.1101/806885; this version posted October 17, 2019. The copyright holder for this preprint (which was not certified by peer review) is the author/funder. All rights reserved. No reuse allowed without permission.

While cell width and length are thought to be regulated by distinct molecular mechanisms, previous studies have also indicated that they are somewhat inter-connected. In a non-essential gene knockout library, the mutants exhibited variation in both mean cell width and length, with a positive correlation between width and length[19]. Similarly, single point mutations in the MreB protein can alter both width and length[20,21], yet a large library of mutants were found to all occupy a specific region of the space of cell geometries during growth in LB in which both wider and thinner mutants had longer mean lengths compared to wildtype[10]. Therefore, cell width and length seem to be regulated by an upstream process which unifies the two aspects of cell shape. In a previous study, it was shown that the regulation of surface area to volume ratio (SA/V) is such a process upstream of cell width and length determination: switching cells at steady-state to a condition in which only cell wall (i.e. surface area) synthesis is partially inhibited increased both cell width and length, which lowers the SA/V[22]. Similarly, SA/V changes during the different stages of growth, with log-phase cells having lower SA/V compared to those in stationary phase[22]; those measurements were performed in highly controlled microfluidic chambers, and cells took tens of minutes to several hours to fully adapt to the new steady-state morphology after the almost instantaneous medium switch. The more continuous changes that cells undergo in a dynamic environment such as batch culture have yet to be fully understood, particularly from the perspective of cellular dimensions.

bioRxiv preprint doi: https://doi.org/10.1101/806885; this version posted October 17, 2019. The copyright holder for this preprint (which was not certified by peer review) is the author/funder. All rights reserved. No reuse allowed without permission.

96

97 In this study, based on precise and frequent experimental measurements of cellular
98 dimensions and growth rates of a batch culture constantly experiencing nutrient
99 compositional changes and waste accumulations, we develop a model that
100 quantitatively predicts SA/V dynamics. Our model predicts a time delay between
101 surface area and volume synthesis adaptation, and that cells outgrowing from
102 stationary phase will always experience a period of active width increase due to optimal
103 resource allocation to volumetric growth. This model focuses on global resource
104 constraints rather than specific molecular machineries, and therefore is broadly
105 applicable to other microbial batch cultures. Indeed, we found that the observed SA/V
106 dynamics are qualitatively universal across microbial species and growth conditions.
107 With only a single free parameter, our time-delay model predicts the SA/V changes due
108 to perturbations in cell-wall synthesis or protein translation. Our work highlights the
109 ability of bacterial cells to rapidly respond to changing environments by modifying
110 their physical growth.

bioRxiv preprint doi: https://doi.org/10.1101/806885; this version posted October 17, 2019. The copyright holder for this preprint (which was not certified by peer review) is the author/funder. All rights reserved. No reuse allowed without permission.

Results

A time-delay model explains the relative dynamics of surface area and volume synthesis in batch cultures

In previous studies, we showed that as *Escherichia coli* cells transition from stationary phase to log phase and back to stationary phase in a batch culture, cellular dimensions vary along with the instantaneous growth rate[9,10]. After a 1:200 back-dilution of an overnight culture grown in LB into fresh LB, cells resumed growth and reached their maximum growth rate after ~1.5 h, after which growth rate gradually slowed down to approximately zero by ~4-5 h (Figure 1A). To validate our previous measurements, we extracted a small sample of cells every 15 min and quickly spotted them onto agarose pads for single-cell imaging and quantification (Methods). Mean cell length increased only slightly in the first 0.5 h. The peak in bulk growth rate at 1.5 h corresponded with the peak in mean cell length across the population (Figure 1B), which increased by ~3-fold relative to stationary phase cells. The mean cell width increased linearly immediately after dilution, and reached its maximum after ~1 h, increasing by ~25% relative to stationary phase cells (Figure 1B). Since both length and width initially increase, the surface area-to-volume ratio (SA/V) decreased over this time; SA/V reached its minimum at approximately the same time as the peak in growth rate and mean length (1.5 h; Figure 1C). After 1.5 h, the dynamics of length, width, and SA/V

bioRxiv preprint doi: https://doi.org/10.1101/806885; this version posted October 17, 2019. The copyright holder for this preprint (which was not certified by peer review) is the author/funder. All rights reserved. No reuse allowed without permission.

were more gradual, with all quantities reaching plateaus by 5 h. We term these measurements of cell dimensions throughout a passage cycle as a "shape growth curve," by analogy to absorbance measurements. Using such measurements, we can accurately capture single-cell shape dynamics in a liquid batch culture over extended time periods.

To confirm that the observed changes in cellular dimensions and SA/V were not due to artifacts of sampling, we performed time-lapse imaging by diluting and spotting stationary phase cells onto agarose pads containing fresh medium, and tracked the same cells for 1.5 h as they resumed growth on pads. The growth rates of these cells mimicked a population grown in liquid culture, and their shape dynamics recapitulated the shape growth curves (Figure 1D). In particular, each single cell immediately increased in width as soon as it was placed on the agarose pad with fresh medium, while length did not increase noticeably until 20-30 min later (Figure 1D). Therefore, our shape growth curves indeed reflect the morphological changes for each single cell in the batch culture.

Previous work showed that if surface area synthesis, like volume synthesis, is dependent on cell volume (rather than surface area), SA/V will equilibrate at a steady-state value corresponding to the ratio of surface and volume synthesis rates[22] (Figure

bioRxiv preprint doi: https://doi.org/10.1101/806885; this version posted October 17, 2019. The copyright holder for this preprint (which was not certified by peer review) is the author/funder. All rights reserved. No reuse allowed without permission.

1E). Our measurements for cells transitioning out of and into stationary phase are clearly not at steady state as growth rate is constantly changing, and indeed mean SA/V varied by ~25%. If we extend the exponential growth laws[22] for volume V, $\frac{dV}{dt} = \alpha V(t)$, and surface area A, $\frac{dA}{dt} = \beta V(t)$, to now cover non-exponential growth through time-dependent functions $\alpha(t)$ and $\beta(t)$, we can derive (Figure 1E) an equation for the dynamics of A/V:

$$\frac{d\left(\frac{A}{V}\right)}{dt} = \frac{1}{V}\frac{dA}{dt} - \frac{A}{V^2}\frac{dV}{dt} = \beta(t) - \alpha(t)\frac{A}{V}. \qquad (3)$$

At steady-state, $\frac{d\left(\frac{A}{V}\right)}{dt} = 0$, and therefore $\frac{A}{V} = \frac{\beta}{\alpha}$. Previous studies have measured these steady-state SA/V values across media that support different growth rates α, showing that steady-state SA/V was approximately linear (with negative slope) as a function of α[6]. Hence, we approximated β as a hyperbolic function of α based on our steady-state SA/V measurements (Methods), providing an empirical relationship $\beta(t) = f\left(\alpha(t)\right)$. With our measured value of initial SA/V at t=0, the dynamics of α (calculated from optical density readouts), and the function f, we obtained a prediction for the SA/V dynamics during a shape growth curve (Figure S1A), and found that the model poorly predicted our experimental measurements. Specifically, the model predicted a slower initial decrease in SA/V, and the minimum value was higher and occurred at a later time than our experimental measurements. The final SA/V value never recovered to the initial value, even though the growth rate α was 0 at the beginning and end. Thus, the

bioRxiv preprint doi: https://doi.org/10.1101/806885; this version posted October 17, 2019. The copyright holder for this preprint (which was not certified by peer review) is the author/funder. All rights reserved. No reuse allowed without permission.

model based on a quasi-steady state assumption does not capture some key factor(s) contributing to the SA/V changes during batch culturing.

Studies focused on the *E. coli* proteome have shown that conditions that support higher growth rate require a reallocation of protein synthesis toward ribosomes[7,8]. We hypothesized that the transition from stationary phase to log growth would require a similar shift in proteome composition more heavily weighted toward cytoplasmic components than surface area components (Figure 1F), which could lead to different temporal dynamics between α and β contrary to the quasi-steady state hypothesis. To explore such a possibility, we analyzed our single-cell time-lapse trajectories (Figure 1D) to measure α and β for each cell. From our measurements of α, we calculated $f(\alpha)$, the expected value of β during steady-state growth at rate α. We found that $f(\alpha)$ increased more quickly than β, with a roughly constant time delay of ~10 min between the two curves (Figure 1G). Thus, we modified our model in Eq. 3 by substituting the function between α and β to be $\beta(t) = f\big(\alpha(t-\Delta t)\big)$, where Δt is a constant that characterizes the time delay between β and α. Fitting our experimental data with the time-delay model yielded almost perfect agreement with a time delay $\Delta t = 11$ min (Figure 1H). Thus, the minimal time-delay model with a single free parameter is able to almost entirely recapitulate the quantitative features of SA/V dynamics.

bioRxiv preprint doi: https://doi.org/10.1101/806885; this version posted October 17, 2019. The copyright holder for this preprint (which was not certified by peer review) is the author/funder. All rights reserved. No reuse allowed without permission.

To confirm that such a delay actually occurs, we utilized a library of *E. coli* strains with GFP reporting the expression from various promoters[23] and sought to directly quantify the dynamics of cytoplasmic and surface-related proteins as cells emerge from stationary phase. We tested two strains representing ribosomal proteins (P_{rplL}-GFP, P_{rpsU}-GFP), two representing other cytoplasmic proteins (P_{lacI}-GFP, P_{gyrB}-GFP), and two representing enzymes related to cell-wall synthesis (P_{mrcB}-GFP, P_{murA}-GFP). We grew each strain in LB overnight to saturation, then placed the cells directly into a microfluidic device surrounded by the supernatant from the overnight culture. We then switched the spent medium to fresh LB and monitored cell morphology and gene expression. In all six strains, GFP levels increased during growth, signifying increased expression. Consistent with our model prediction, the promoters of cytoplasmic proteins increased expression faster than those of the cell-wall genes (Figure 1I). We quantified the expression dynamics by calculating t_{10}, the time for each promoter to increase their relative expression by 10% (a proxy for promoter activation). The promoters for cytoplasmic proteins had $t_{10} \sim 10$ min, whereas the promoters for cell-wall enzymes had $t_{10} \sim 20$ min, a delay of $\Delta t \sim 10$ min. Therefore, our direct measurement of gene expression dynamics confirmed a delay between α and β, indicating differential regulation of the proteome (Figure 1F).

bioRxiv preprint doi: https://doi.org/10.1101/806885; this version posted October 17, 2019. The copyright holder for this preprint (which was not certified by peer review) is the author/funder. All rights reserved. No reuse allowed without permission.

209 Our ability to fit the complex SA/V dynamics during batch culture with a simple model
210 involving only the introduction of a time delay to the steady-state relationship between
211 β and α suggests a simple picture of the initial stages of growth: as cells emerge from
212 stationary phase, they devote more resources to synthesizing cytoplasmic components
213 such as ribosomes than to surface components such as the cell wall. While the cell still
214 must expand to allow space for these new cytoplasmic components, it does so with a
215 minimal amount of surface growth by expanding predominantly in width rather than
216 length, as volume scales approximately quadratically with width but only linearly with
217 length. Indeed, in a typical rod-shaped cell, a two-fold change in volume requires only a
218 47% increase in surface area if cells only increase in width, but 91% if cells increase only
219 in length (Figure 1J, Methods). To test this reasoning, from our single-cell time-lapse
220 results (Figure 1D), we directly calculated the possible range of β at each time point
221 using the observed width, length and growth rate α (Methods). At $t = 0$, the measured β
222 was close to its minimal possible value, characterizing a widening-dominant growth
223 mode. By $t = 60$ min, the measured β approximately reached its maximum under those
224 growth conditions, consistent with the canonical elongation-dominant growth mode
225 (Figure 1K). Thus, during outgrowth from stationary phase, cells transition their growth
226 mode from widening to elongation.
227

bioRxiv preprint doi: https://doi.org/10.1101/806885; this version posted October 17, 2019. The copyright holder for this preprint (which was not certified by peer review) is the author/funder. All rights reserved. No reuse allowed without permission.

228 **Cell widening during exit from stationary phase occurs even if width decreases at**
229 **steady-state**

230 To further validate that the initial increase in width during outgrowth from stationary
231 phase (Figure 1B,D,K) is governed by the delay between α and β, rather than
232 determined solely by the current nutrient condition after back dilution, we took
233 stationary-phase cells grown in LB and diluted them into M9 glucose medium. Cells
234 grown in LB always had widths larger than 0.94 μm (Figure 1B), whereas cell widths
235 during passage exclusively in M9 glucose never exceeded 0.94 μm (Figure S1B). Thus, if
236 the medium cells are diluted into dictated cell shape, cell width in M9 glucose would
237 only decrease to below 0.94 μm. However, we observed that by 30 min after dilution
238 into M9 glucose from a stationary-phase LB culture, cell width increased by ~8% and
239 reached ~1.03 μm (Figure 1L), a value that was not achievable for cells always passaged
240 in M9 glucose (Figure S1B). Afterward, cell width dropped to ~0.9 μm, as expected for
241 cells passaged in M9 glucose (Figure S1B), which we presume is mainly dictated by the
242 M9 medium. Therefore, the initial widening of cells during outgrowth is not
243 determined by external nutrients.

244

245 Outgrowth from stationary phase also involves changes such as altered expressions of
246 stress-response genes, initiation of DNA replication, and different osmolalities of fresh
247 versus stationary phase media. We tested these possibilities by repeating shape growth

bioRxiv preprint doi: https://doi.org/10.1101/806885; this version posted October 17, 2019. The copyright holder for this preprint (which was not certified by peer review) is the author/funder. All rights reserved. No reuse allowed without permission.

curve measurements in a ppGpp^0 strain and a Δ*thyA* strain. The ppGpp^0 strain is unable to synthesize ppGpp, a small nucleotide regulating stress-related genes[1]. The Δ*thyA* strain does not replicate DNA in the absence of external thymine[24]. In both strains, shape growth curves still exhibited similar outgrowth dynamics (Supplementary Text, Figure S1C-J). Systematically tuning the osmolality of media caused much smaller shape changes than those observed in the shape growth curves (Supplementary Texts, Figure S1K). Taken together, we conclude that the initial increase in width is likely governed by proteome re-allocation rather than external factors or other biological processes.

Cells exiting from stationary phase reach a critical SA/V at their first division

Previous work suggested that exponentially growing cells accumulate excess surface area material during the cell cycle, which then triggers division[22]. For a rod-shaped cell, division adds two hemispheric poles and increases SA by 4% without changing volume (Figure S2A). Since cells decrease their SA/V during outgrowth (Figure 1D), we thus asked whether the first division after cells exit from stationary phase was also related to their SA/V.

We diluted stationary-phase cells and placed them onto an agarose pad containing fresh LB, tracked single cells until their first division, and quantified their cellular

bioRxiv preprint doi: https://doi.org/10.1101/806885; this version posted October 17, 2019. The copyright holder for this preprint (which was not certified by peer review) is the author/funder. All rights reserved. No reuse allowed without permission.

dimensions. Several models have been proposed for cell-size control during steady-state growth: the "sizer" model, in which cells divide at a fixed size; the "adder" model, in which cells add a fixed volume before division; and the "timer" model, in which cells grow for a fixed time before division[25]. The "sizer" model predicts that the volume at division is independent of initial volume, while the "adder" model predicts a slope of +1 between volume at division and initial volume. During outgrowth from stationary phase, we found that the volume at the first division negatively correlated with the initial volume (Figure 2A), deviating from both the sizer and adder models. Similar negative correlations were observed for cell length and surface area (Figure S2B,C). The timer model also failed to explain the data, with time to first division negatively correlated with initial cell volume (Figure 2B). However, the SA/V at division was approximately constant and independent of the initial SA/V (Figure 2C). Moreover, the normalized distribution of SA/V at division was much narrower compared to other cellular dimensions (Figure 2C,D), suggesting that the first division after stationary-phase exit is linked to a critical SA/V.

We further asked how division-related proteins were regulated during stationary-phase exit by tracking the dynamics of the key division protein FtsZ. We selected four *E. coli* strains, each containing a mutation in the actin homolog MreB that exhibited different mean widths and lengths during log-phase growth [10]. These mutants allowed us to

bioRxiv preprint doi: https://doi.org/10.1101/806885; this version posted October 17, 2019. The copyright holder for this preprint (which was not certified by peer review) is the author/funder. All rights reserved. No reuse allowed without permission.

analyze division dynamics in cells of different widths. These strains also contained a chromosomally-integrated internal fusion of FtsZ to monomeric Venus (FtsZ^{sw}-mVenus) at the native FtsZ locus[10,26], allowing quantification of FtsZ abundance using fluorescence microscopy (Methods). All strains exhibited qualitatively similar cell shape dynamics as wild-type *E. coli*, despite their altered lengths and widths (Figure S2D,E,F). Total FtsZ fluorescence remained constant in the first 45 min post-dilution before starting to increase (Figure 2E), indicating that FtsZ synthesis started much later compared to other genes (Figure 1I). We also measured FtsZ dynamics in a time-lapse experiment with GFP fused to the FtsZ promoter (P_{ftsZ}-GFP)[23] and confirmed that FtsZ expression started ~50 min post-dilution (Figure S2G). Although the four MreB mutants had different levels of total FtsZ (Figure 2E), FtsZ concentration was quantitatively similar across the different strains (Figure 2E, inset), suggesting a conserved mechanism of FtsZ regulation independent of cell shape, consistent with previous measurements in exponential-phase cells[10]. In all strains, no FtsZ rings were observed until ~50 min post-dilution. Virtually all cells contained one FtsZ ring by ~100 min post-dilution (Figure 2F), consistent with the observed timing of the first division after stationary-phase exit (Figure 2B). Taken together, these data indicate that FtsZ levels are upregulated concurrent with the need for division.

SA/V dynamics are broadly conserved across width and length perturbations

bioRxiv preprint doi: https://doi.org/10.1101/806885; this version posted October 17, 2019. The copyright holder for this preprint (which was not certified by peer review) is the author/funder. All rights reserved. No reuse allowed without permission.

Since SA/V is dependent on both cell width and length, we asked whether chemically or genetically tuning cell width or length would affect SA/V dynamics. We first treated wild-type *E. coli* cells with a range of concentrations of cephalexin, a β-lactam antibiotic that inhibits the division-specific cell-wall synthesis enzyme PBP3[27]. Importantly, lower cephalexin concentrations (2.5 μg/mL and 5 μg/mL) did not affect bulk growth rate for at least the first 10 h of growth. For the highest cephalexin concentration used (10 μg/mL), cells started to lyse after 2 h, but growth was not affected prior to lysis (Figure S2H). Thus, cephalexin treatment does not directly affect any parameters in our model, despite the obvious perturbations in cell length. Shape growth curves showed that cells became longer due to inhibition of cell division in a concentration-dependent manner (Figure 2G). However, as cephalexin concentration was increased, cell width peaked at a lower value and began to decrease at an earlier time point (Figure 2H). As a result, SA/V was maintained throughout the first 3 h (Figure 2I) despite the marked changes in cell length. Therefore, cells collectively regulate width and length to maintain SA/V during growth.

We further studied cell shape changes in a library of *E. coli* mutants with a wide range of mean cell lengths and widths[10]. While the strains had different morphologies, they all exhibited similar SA/V dynamics as observed in wild-type *E. coli* (Supplementary Text,

bioRxiv preprint doi: https://doi.org/10.1101/806885; this version posted October 17, 2019. The copyright holder for this preprint (which was not certified by peer review) is the author/funder. All rights reserved. No reuse allowed without permission.

Figure S2I-N), further indicating that the SA/V dynamics (Figure 1C) are conserved across genetic perturbations to cellular dimensions.

SA/V dynamics are conserved across species and growth temperatures in rich media

The basis of our interpretation of SA/V dynamics during batch culture should be generally applicable to species other than *E. coli*, as it does not make any assumptions about *E. coli*-specific pathways. Hence, we predicted that a similar initial decrease in SA/V upon outgrowth from stationary phase should generally occur. We thus expanded our shape growth curve measurements to a variety of other species and conditions. We quantified shape growth curves for the Gram-negative bacteria *Vibrio cholerae* and *Caulobacter crescentus*, both of which form slightly curved rods, the rod-shape Gram-positive bacterium *Bacillus subtilis*, and the eukaryote fission yeast *Schizosaccharomyces pombe*. In all species we tested, SA/V dynamics were similar to those in *E. coli*, with SA/V decreasing when cells resumed growth, and then gradually recovering when cell growth slowed down again (Supplementary Text, Figure S3A-E).

Bacterial cell size during steady-state growth is thought to be relatively constant as growth rate changes across temperatures[5]. Nonetheless, we still found that *E. coli* cells at 30, 37, and 42 °C had different cellular dimensions and SA/V values. At all temperatures, cells still obeyed similar SA/V dynamics (Supplementary Text, Figure

bioRxiv preprint doi: https://doi.org/10.1101/806885; this version posted October 17, 2019. The copyright holder for this preprint (which was not certified by peer review) is the author/funder. All rights reserved. No reuse allowed without permission.

S3F,G). Taken together, the initial decreases of SA/V appear to be general across microbial species, growth temperatures, and cell shapes and sizes, indicating that as cells accelerate in growth, volume synthesis always increases more quickly than surface synthesis.

SA/V regulation is dependent on nutrient conditions

We next asked whether medium composition affects SA/V dynamics, considering that steady-state cell shape is nutrient-dependent[6]. We quantified shape growth curves in M9 media supplemented with different carbon/nitrogen sources that support different growth rates. Overall, in low-nutrient conditions with slower growth rates, Δt was close to zero and SA/V remained largely constant, despite substantial changes in cell width and length (Supplementary Text, Figure S4A-E). Richer nutrient conditions supported faster growth rates and led to larger changes in SA/V and non-zero Δt values (Supplementary Text, Figure S4F-H). Since cell shape changes occurred even in defined media with a single carbon source (Figure S4C,D), the observed cellular dimension changes across shape growth curves are not likely due to diauxic shifts caused by nutrient consumption, but rather related to the dynamics of proteome composition as growth rate changes. A more complex panel of nutrients that support faster growth likely requires a larger shift in proteome composition (Figure 1F), driving a larger range of SA/V changes (Figure S4I).

bioRxiv preprint doi: https://doi.org/10.1101/806885; this version posted October 17, 2019. The copyright holder for this preprint (which was not certified by peer review) is the author/funder. All rights reserved. No reuse allowed without permission.

367

368 **Time-delay model quantitatively predicts SA/V decreases due to inhibiting cell-wall**
369 **synthesis**

370 We next sought to test predictions of our time-delay model experimentally. In our
371 model, reducing β (without changing α) predicted that the shape growth curve would
372 exhibit larger SA/V decreases during the first 2 h, with a final SA/V when cells returned
373 to stationary phase lower than the initial value (Figure 3A). The *E. coli* cytoplasm is
374 surrounded by the cell envelope, constituted of three layers: the cell wall, and two
375 membranes on either side of the cell wall. The cell wall mainly consists of
376 peptidoglycan, and the membranes are constituted by lipids, proteins, and
377 lipopolysaccharides. Since in most conditions the synthesis of peptidoglycan is more
378 energetically costly compared to lipids[28], we hypothesized that that altering cell-wall
379 synthesis would have a larger effect on β.

380

381 To validate our model prediction, we treated cells with multiple antibiotics that inhibit
382 cell-wall synthesis and asked whether the SA/V changes were consistent with the model
383 predictions. We first treated MG1655 cells grown in LB with A22[29], a small molecule
384 inhibiting the actin homolog MreB and therefore affecting the spatial pattern of new cell
385 wall incorporation. Sub-lethal concentrations of A22 did not affect growth rate during
386 the first 3 h of growth, but cells treated with A22 exhibited dose-dependent increases in

bioRxiv preprint doi: https://doi.org/10.1101/806885; this version posted October 17, 2019. The copyright holder for this preprint (which was not certified by peer review) is the author/funder. All rights reserved. No reuse allowed without permission.

387 cell width compared to the non-treated control (Figure S5A), as previously shown [30].
388 Interestingly, the increase in cell width was accompanied by relatively lower increases
389 in cell length (Figure S5B), which partially compensated for the decrease in SA/V.
390 Together, the inhibition of cell-wall synthesis by A22 caused SA/V to drop in a dose-
391 dependent fashion (Figure 3B), as predicted by our model (Figure 3A). Fitting the A22
392 shape growth curves to our model was indeed consistent with a dose-dependent
393 decrease β (Figure 3B). Δt was not affected except at the highest A22 concentration,
394 which resulted in a ~50% longer time delay (Table S2), presumably because higher A22
395 concentrations require further proteome redistribution. We also tested two other cell-
396 wall synthesis inhibitors, fosfomycin and mecillinam. Fosfomycin inhibits MurA, the
397 enzyme catalyzing the first committed step of peptidoglycan biosynthesis[31,32], and
398 mecillinam specifically targets PBP2, a transpeptidase that crosslinks new cell-wall
399 material[33]. In both cases, we observed similar changes to shape growth curves as with
400 A22 treatment (Figure S5C,D).
401
402 Since cells grown in M9 glucose exhibited largely constant SA/V and virtually no time
403 delay (Figure S4A), we asked whether inhibiting SA synthesis would affect their SA/V
404 dynamics by treating cells grown in M9 glucose with A22. In this case, A22 also caused
405 a similar drop in SA/V (Figure 3C) and mean length (Figure S5E), and cell width now
406 increased as opposed to the slight decrease in the A22-free control (Figure S5F). Thus,

bioRxiv preprint doi: https://doi.org/10.1101/806885; this version posted October 17, 2019. The copyright holder for this preprint (which was not certified by peer review) is the author/funder. All rights reserved. No reuse allowed without permission.

the relatively small range of SA/V changes observed in M9 glucose (Figure S4A) was indeed because the proteome composition for surface area and volume synthesis was largely balanced in M9 glucose. Nonetheless, perturbations such as A22 treatment can still break this proteome balance and alter SA/V more substantially. Fitting the A22 SA/V dynamics to our model also showed that at high A22 concentrations, in addition to decreased β (Table S2), Δt became non-zero (Figure 3C), suggesting that cells have to re-allocate their proteome composition to accommodate inhibition of cell-wall synthesis.

Cell wall synthesis can also be altered genetically. In *V. cholerae*, activation of a histidine kinase/response regulator two-component system, WigK/WigR, increases expression of many cell-wall synthesis genes and elevates cell-wall synthesis[34]. We therefore quantified the shape growth curves of *V. cholerae* strains with a range of cell-wall synthesis capacities. Compared to wildtype, overexpression of WigR increased SA/V (Figure 3D), mainly through decreased cell width. Overexpression of $WigR^{D78E}$, a phosphomimetic version of WigR, further increases cell wall synthesis[34], and SA/V increased even more as expected (Figure 3D), accompanied by further decreases in cell width. By contrast, deletion of WigR slows down cell wall synthesis, and we observed decreases in SA/V similar to those during treatment of *E. coli* with wall-acting antibiotics (Figure 3D). Therefore, genetically perturbing cell-wall synthesis affects β and therefore SA/V dynamics as predicted by our model.

bioRxiv preprint doi: https://doi.org/10.1101/806885; this version posted October 17, 2019. The copyright holder for this preprint (which was not certified by peer review) is the author/funder. All rights reserved. No reuse allowed without permission.

We next tested whether inhibiting lipid synthesis would have similar effects on SA/V dynamics. While it has been previously shown that inhibiting fatty acid synthesis via treatment with cerulenin alters cell morphology[35], those experiments were performed in a regime (cerulenin concentration >50 μg/mL) in which growth rates were strongly affected (Figure S5G). In the context of our model, at lower concentrations of cerulenin (<10 μg/mL) where growth rates remained unaffected (Figure S5G), we did not observe noticeable changes in cellular dimensions after 2 h of growth (Figure S5H). Similarly, in cell wall-deficient spheroplasts[36], surface area was only limited by lipid synthesis, and those cells exhibited increased, rather than decreased, SA/V during outgrowth from stationary phase (Supplementary Text, Figure S5I). We further analyzed previously published proteome datasets[11,37], and found that levels of lipid synthesis proteins, but not peptidoglycan synthesis proteins, increased monotonically with growth rate (Supplementary Text, Figure S5J-L). Taken together, lipid biosynthesis protein levels are likely directly linked to growth rate, and cell envelope growth is limited by cell wall rather than membrane synthesis.

Inhibiting translation increases the time delay between volume and surface growth

The addition of the time delay Δt was a critical modification to our model in order to fit our experimental shape growth curve data (Figure 1H, Figure S1A). We therefore asked

bioRxiv preprint doi: https://doi.org/10.1101/806885; this version posted October 17, 2019. The copyright holder for this preprint (which was not certified by peer review) is the author/funder. All rights reserved. No reuse allowed without permission.

447 whether modifying Δt would have observable effects on SA/V dynamics. By increasing
448 Δt from 11 to 25 min, our model predicted that the minimal SA/V reached in log phase
449 would decrease, while the final SA/V when cells enter stationary phase would increase
450 (Figure 4A). Such non-monotonic changes to SA/V dynamics are somewhat counter
451 intuitive, highlighting the biological relevance of the time delay. The initial SA/V drop
452 after exiting stationary phase is primarily due to the quick increase in α. While β also
453 increases, the time delay between α and β causes V to grow faster than A, leading to
454 decreased SA/V. Therefore, a larger Δt means that V increases more before A growth
455 catches up, resulting in an even lower SA/V in log phase. As for the terminal SA/V, it is
456 dependent on $\frac{\int dA/dt}{\int dV/dt}$, an integral effect that depends on the entirety of the growth
457 dynamics. $\frac{dV}{dt}$ only depends on α and remains unaffected, while $\frac{dA}{dt} = \beta V(t) =$
458 $f\big(a(t-\Delta t)\big)V(t)$. Increasing Δt leads to increased $\int dA/dt$ and eventually a higher
459 terminal SA/V.
460
461 We tested these predictions by treating cells with low levels of chloramphenicol, a
462 translational inhibitor, based on our inference that Δt is mainly determined by rates of
463 proteome re-allocation (Figure 1F). Although inhibiting protein translation inevitably
464 affected both α and β, at very low chloramphenicol concentrations (~0.01-0.05X minimal
465 inhibitory concentration), cell growth was largely unaltered, and the SA/V dynamics
466 matched our model predictions: increasing chloramphenicol concentrations increased

bioRxiv preprint doi: https://doi.org/10.1101/806885; this version posted October 17, 2019. The copyright holder for this preprint (which was not certified by peer review) is the author/funder. All rights reserved. No reuse allowed without permission.

467 Δt by ~70%, while β only changed <5% across conditions (Figure 4B). In these cases, the
468 changes in SA/V were largely dictated by the relatively larger cell widths under
469 chloramphenicol treatment (Figure S6A), as cell length followed very similar trends
470 across concentrations (Figure S6B). Higher chloramphenicol concentrations
471 substantially reduced growth rate and led to even lower SA/V in log phase (Figure
472 S6C). Model fitting found that the reduced SA/V was also mainly due to increased Δt
473 (Figure S6C), as β changed less than 10% (Table S2). Thus, our shape growth curves
474 with chloramphenicol treatment provide further validation of our model predictions,
475 and demonstrate that tuning Δt has observable effects, rather than merely acting as a
476 fitting parameter.
477

bioRxiv preprint doi: https://doi.org/10.1101/806885; this version posted October 17, 2019. The copyright holder for this preprint (which was not certified by peer review) is the author/funder. All rights reserved. No reuse allowed without permission.

Discussion

Although much work has been done to unveil the molecular players determining cell morphology at steady states, an approach unifying cell morphology and growth rates in dynamic environments is still lacking. In this study, our time-delay model of SA/V dynamics accurately predicted how cell size responded to growth rate changes, and was generally applicable across many species and growth conditions. The minimal assumption of a single, constant time delay between volume and surface area synthesis quantitatively recapitulated the complex SA/V dynamics (Figure 1C, S3, S4), and predicted SA/V changes under perturbations (Figure 3, 4). While previous studies have shown that cells adopt different steady-state SA/V values across growth conditions[6,22], our work further reveals that the quantitative dynamics of SA/V under environmental perturbations are based on global resource allocation and the temporal dependence between surface area and volume growth (Figure 1I). Our model thus has the potential to quantitatively describe other dynamic biological processes that scale with cell volume[38].

While we obtained the time delay between surface area and volume synthesis (Δt) via model fitting, systematically tuning Δt conferred non-monotonic changes in SA/V dynamics (Figure 4A,B), highlighting its biological relevance. Indeed, we were able to

bioRxiv preprint doi: https://doi.org/10.1101/806885; this version posted October 17, 2019. The copyright holder for this preprint (which was not certified by peer review) is the author/funder. All rights reserved. No reuse allowed without permission.

quantify the delay of surface area growth compared to volumetric growth by directly tracking protein expression in single cells (Figure 1G), and the delay was observed previously when cells were switched from one steady state to another[22]. Inhibiting protein translation increased Δt (Figure 4B), suggesting that surface area synthesis was delayed due to a slower regulation of surface area synthesis-related enzymes. The connection between Δt and changes in growth rate is complex, since higher growth rates may require larger shifts in proteome, but also speeds up proteome turnover. Thus, Δt does not necessarily have a simple correlation with growth rates. Other factors, such as cell-wall precursor synthesis and insertion, could also alter Δt in addition to proteome changes. It remains to be explored why and how surface area and volume synthesis rates are differentially modulated, and the ways in which such a delay can be beneficial for cells.

Our model predicts that upon growth resumption, cells should always increase in width, as surface area synthesis is limiting and increasing width rather than length poses a lower demand for surface area material (Figure 1J). We observed such width increases after diluting stationary-phase cells into fresh media across all species and experimental conditions (Figure 1B,D,L, S3, S4). Similar changes in width have been reported in growth-inhibited cells due to the presence of an antibiotic, in which *E. coli* cells resumed growth after washing out the antibiotic and cell width increased prior to

bioRxiv preprint doi: https://doi.org/10.1101/806885; this version posted October 17, 2019. The copyright holder for this preprint (which was not certified by peer review) is the author/funder. All rights reserved. No reuse allowed without permission.

length increase[39]. The initial widening of cells is likely related to active growth and the subsequent imbalance between surface area and volume synthesis. In *E. coli*, such widening has been linked to altered cell wall insertion patterns governed by changes in MreB localization patterns[9,10], providing a potential molecular mechanism in response to limited surface area synthesis. While DNA replication is a central process in cell proliferation and has implications in cell-size determination[6,40], we have shown that cell shape remodeling can be independent of DNA replication (Figure S1G-J), at least in the initial 2 h of shape growth curves, indicating that the effect of DNA abundance on cell shape potentially manifests on a different time scale or is growth dependent. Regardless, our findings strongly suggest that the dynamic coordination between surface area and volume growth dictates cell shape.

E. coli cell division at steady state is well described by the adder model[41]. However, for cells growing out of stationary phase, we observed that cells did not add a constant volume, surface area, or length (Figure 2A, Figure S2B,C), nor did they divide at a fixed size or after a fixed time interval (Figure 2A,B). Instead, cell division occurred at a given SA/V (Figure 2C,D), highlighting the biological relevance of SA/V regulation. The key division protein, FtsZ, was upregulated concurrently with the need for cell division (Figure 2E,F, S2G), consistent with previous work showing that a threshold of FtsZ is required for cell division[42,43]. The dynamics of FtsZ were further delayed compared to

bioRxiv preprint doi: https://doi.org/10.1101/806885; this version posted October 17, 2019. The copyright holder for this preprint (which was not certified by peer review) is the author/funder. All rights reserved. No reuse allowed without permission.

538 other cell-wall synthesis genes (Figure 1I, S2G), reinforcing the idea that gene
539 expression during growth resumption is temporally regulated to allow cells to prioritize
540 volumetric growth over surface area synthesis or division.
541
542 Our model of SA/V dynamics links cell width and length, even though the two
543 dimensions are regulated by distinct molecular machineries[14,15,33]. Interestingly,
544 perturbations known to increase cell width or length also led to decreases in the other
545 dimension (Figure 2G,H, S5A,B,E,F). Larger cell width and length both decrease SA/V,
546 and a corresponding decrease in cell length or width can compensate for an increase in
547 the other to maintain SA/V. Therefore, despite the seemingly disjoint nature of cell
548 width and length regulation in rod-shaped cells, the global resource limitation on
549 surface area growth poses constraints on the two dimensions. From an evolutionary
550 perspective, bacterial cells constantly encounter feast or famine conditions, and
551 therefore optimize the resource allocation strategies through regulations between
552 surface area and volume growth. Rod-like shapes allow cells to efficiently tune SA/V via
553 two disparate growth modes (Figure 1J), which potentially confers evolutionary
554 benefits compared to other shapes. In eukaryotic cells, a nuclear transporter receptor
555 serves as a sensor of SA/V[44], and it remains to be discovered whether similar global
556 SA/V sensors exist in bacterial cells, which would provide opportunities to reveal new

bioRxiv preprint doi: https://doi.org/10.1101/806885; this version posted October 17, 2019. The copyright holder for this preprint (which was not certified by peer review) is the author/funder. All rights reserved. No reuse allowed without permission.

557 connections between cell physiology, size, and fundamental mechanisms of

558 morphogenesis.

559

bioRxiv preprint doi: https://doi.org/10.1101/806885; this version posted October 17, 2019. The copyright holder for this preprint (which was not certified by peer review) is the author/funder. All rights reserved. No reuse allowed without permission.

Methods

Strains and media

Strains used in this study are described in Table S1. For routine culturing, all cells were grown in lysogeny broth (LB) at 37 °C unless otherwise specified. *C. crescentus* cells were grown in PYE (peptone-yeast extract) media at 30 °C as previously described[22], and *S. pombe* cells were grown in YES255 media at 30 °C. Antibiotics (Sigma Aldrich, St. Louis, MO, USA) were used at the concentrations noted in the text. IPTG was used at a final concentration of 1 mM for *V. cholerae* cells. Thymine was added at a final concentration of 500 μg/mL for the *E. coli* Δ*thyA* strain. For minimal media, glucose or other carbon sources were added at final concentration of 0.4%, six amino acids (L-methionine, L-histidine, L-arginine, L-proline, L-threonine, and L-tryptophan) were added to final concentrations of 500 μg/mL each, and casamino acids were added to a final concentration of 3% (w/v).

Strains were inoculated from freezer stocks into test tubes with 3 mL of media and supplemented with the appropriate antibiotics. The tubes were incubated overnight, except for cells grown in M9 acetate, which were incubated for 48 hours. Overnight cultures were back-diluted 1:200 into the same fresh medium for shape growth curves and growth curves measurements.

bioRxiv preprint doi: https://doi.org/10.1101/806885; this version posted October 17, 2019. The copyright holder for this preprint (which was not certified by peer review) is the author/funder. All rights reserved. No reuse allowed without permission.

Spheroplasts were grown in LFLB (LB with additional 3.6% sucrose and 10 mM $MgSO_4$) at 30 °C, with 60 μg/mL cefsulodin added to inhibit cell wall growth[45]. For shape growth curve measurements, overnight spheroplast cultures with cefsulodin were washed three times in fresh LFLB, and diluted 1:10 into LFLB with or without cefsulodin.

Single-cell imaging

For imaging, samples were taken from test tubes and placed on 1% agarose pads every 15 min, and then imaged within 5 min. For membrane staining, a small aliquot of cells was incubated with FM 4-64 (Invitrogen) at a final concentration of 5 μg/mL for 5 min and spotted on agarose pads without washing. Phase-contrast images and epifluorescence images were acquired with a Nikon Ti-E inverted microscope (Nikon Instruments) using a 100X (NA 1.40) oil immersion objective and a Neo 5.5 sCMOS camera (Andor Technology). The microscope was outfitted with an active-control environmental chamber for temperature regulation (HaisonTech, Taipei, Taiwan). Images were acquired using μManager v.1.4[46].

Morphological analyses

bioRxiv preprint doi: https://doi.org/10.1101/806885; this version posted October 17, 2019. The copyright holder for this preprint (which was not certified by peer review) is the author/funder. All rights reserved. No reuse allowed without permission.

599 The MATLAB (MathWorks, Natick, MA, USA) image processing code *Morphometrics*[19]
600 was used to segment cells and to identify cell outlines from phase-contrast or
601 fluorescence microscopy images. A local coordinate system was generated for each cell
602 outline using a method adapted from *MicrobeTracker*[47]. Cell widths were calculated by
603 averaging the distances between contour points perpendicular to the cell midline,
604 excluding contour points within the poles and sites of septation. Cell length was
605 calculated as the length of the midline from pole to pole. Cell volume and surface area
606 were estimated from the local meshing results.
607
608 **FtsZ fluorescence quantification**
609 Cells with a sandwich fusion of mVenus to FtsZ[26] were imaged in phase contrast and
610 fluorescence using an ETGFP filter. FtsZ fluorescence was quantified by summing the
611 intensity values of each pixel within the cell contour. FtsZ rings were identified as the
612 peak of fluorescence intensity along the cell contour.
613
614 **Population-level growth analyses**
615 To measure growth dynamics, overnight cultures were inoculated into 200 μL of fresh
616 media supplemented with the appropriate antibiotics in a clear 96-well plate. The plate
617 was covered with an optical film, with small holes poked at the side of each well to
618 allow aeration. Incubation and OD measurements were performed with an Epoch 2

bioRxiv preprint doi: https://doi.org/10.1101/806885; this version posted October 17, 2019. The copyright holder for this preprint (which was not certified by peer review) is the author/funder. All rights reserved. No reuse allowed without permission.

plate reader (BioTek) at appropriate temperatures with continuous shaking and OD_{600} measured at 7.5-min intervals. The growth rate was calculated as the slope of ln(OD) with respect to time after smoothing using a moving average filter of window size five.

β as a function of α at steady state

Based on previous steady-state growth rate and SA/V measurements, steady-state SA/V linearly correlates with growth rate[6]. Since steady-state SA/V equals β/α, and growth rate is α, β/α is a linear function of α. Therefore, based on SA/V measurements at two different growth rates, we can fit the function relating β to α. In our measurements in LB, *E. coli* cells approaching stationary phase correspond to $\alpha \sim 0$ and $\beta/\alpha = 5.7\ \mu m^{-1}$. By diluting cells repeatedly, cells reached steady-state morphologies[10] for which $\beta/\alpha = 3.8\ \mu m^{-1}$, and the corresponding $\alpha = 1.7\ h^{-1}$. Thus, in LB, we have $\beta/\alpha = 5.7 - 1.12\alpha$, or $\beta = \alpha(5.7 - 1.12\alpha)$.

SA/V as a function of width and length changes

For calculations in Figure 1J and S2E, a cell with width w and length l was approximated by a cylindrical cell body with radius $r = w/2$ and length $l - 2r$, and hemispherical caps on each end with radius $r = w/2$. In this scenario, the corresponding surface area of the cell is $SA = 2\pi r(l - 2r) + 2 \times 2\pi r^2 = \pi w l$, and the volume is $V = \pi r^2(l - 2r) + 4\pi r^3/3 = \pi w^2 l/4 - \pi w^3/12$. For the initial cell, $w = 1\ \mu m$ and $l = 5\ \mu m$.

bioRxiv preprint doi: https://doi.org/10.1101/806885; this version posted October 17, 2019. The copyright holder for this preprint (which was not certified by peer review) is the author/funder. All rights reserved. No reuse allowed without permission.

639

640 **Calculation of permissible range of β**

641 In rod-shaped cells, given the above equations for V and A, $\frac{dV}{dt} = \left(\frac{\pi}{2}wl - \frac{\pi}{4}w^2\right)\frac{dw}{dt} +$

642 $\frac{\pi}{4}w^2\frac{dl}{dt} = \alpha\left(\frac{\pi}{4}w^2l - \frac{\pi}{12}w^3\right)$, and $\frac{dA}{dt} = \pi l\frac{dw}{dt} + \pi w\frac{dl}{dt} = \beta\left(\frac{\pi}{4}w^2l - \frac{\pi}{12}w^3\right)$. During growth,

643 $\frac{dw}{dt} \geq 0$ and $\frac{dl}{dt} \geq 0$. Solving for the linear optimization with the above constraints gives a

644 permissible range of β that is dependent on w, l, and α, with minimum β corresponding

645 to $\frac{dl}{dt} = 0$, and maximum β corresponding to $\frac{dw}{dt} = 0$.

646

647 **DAPI staining and fluorescence quantification**

648 Cells were grown in the same conditions as in single-cell imaging experiments. At each

649 time point, 1 mL of each sample was taken, pelleted at 6,500 rcf for 1 min, and fixed via

650 resuspension in 500 µL 70% ethanol and incubation for 15 min at room temperature.

651 Cells were then pelleted at 6,500 rcf for 1 min, resuspended in 500 µL PBS, with 4',6-

652 diamidino-2-phenylindole (DAPI) added to a final concentration of 1 µg/mL, and

653 incubated in the dark for 15 min. Cells were washed with PBS twice by pelleting at

654 6,500 rcf for 1 min followed by resuspension. Cells were spotted onto 1% agarose pads

655 and imaged in phase contrast and fluorescence using a DAPI filter. DAPI fluorescence

656 was quantified by summing the intensity values of each pixel within the cell contour,

657 and then normalizing to the corresponding intensity in the control.

bioRxiv preprint doi: https://doi.org/10.1101/806885; this version posted October 17, 2019. The copyright holder for this preprint (which was not certified by peer review) is the author/funder. All rights reserved. No reuse allowed without permission.

658

659 **qPCR**

660 To estimate the relative replication rate of the chromosome, we quantified the copy
661 numbers of 16 genetic loci via qPCR and fitted their log(relative abundance) to their
662 corresponding distances to *terC*, as previously described[18]. The cells were harvested at
663 six different time points (in the overnight culture, and 30, 60, 90, 120, and 150 min after
664 1:200 dilution), and the DNA was extracted using the genomic DNA purification kit
665 (Qiagen). The relative abundances of chromosomal loci were quantified by qPCR, using
666 the EvaGreen qPCR kit (Bio-rad). The qPCR probes used were as previously described[47].

667

bioRxiv preprint doi: https://doi.org/10.1101/806885; this version posted October 17, 2019. The copyright holder for this preprint (which was not certified by peer review) is the author/funder. All rights reserved. No reuse allowed without permission.

Figures

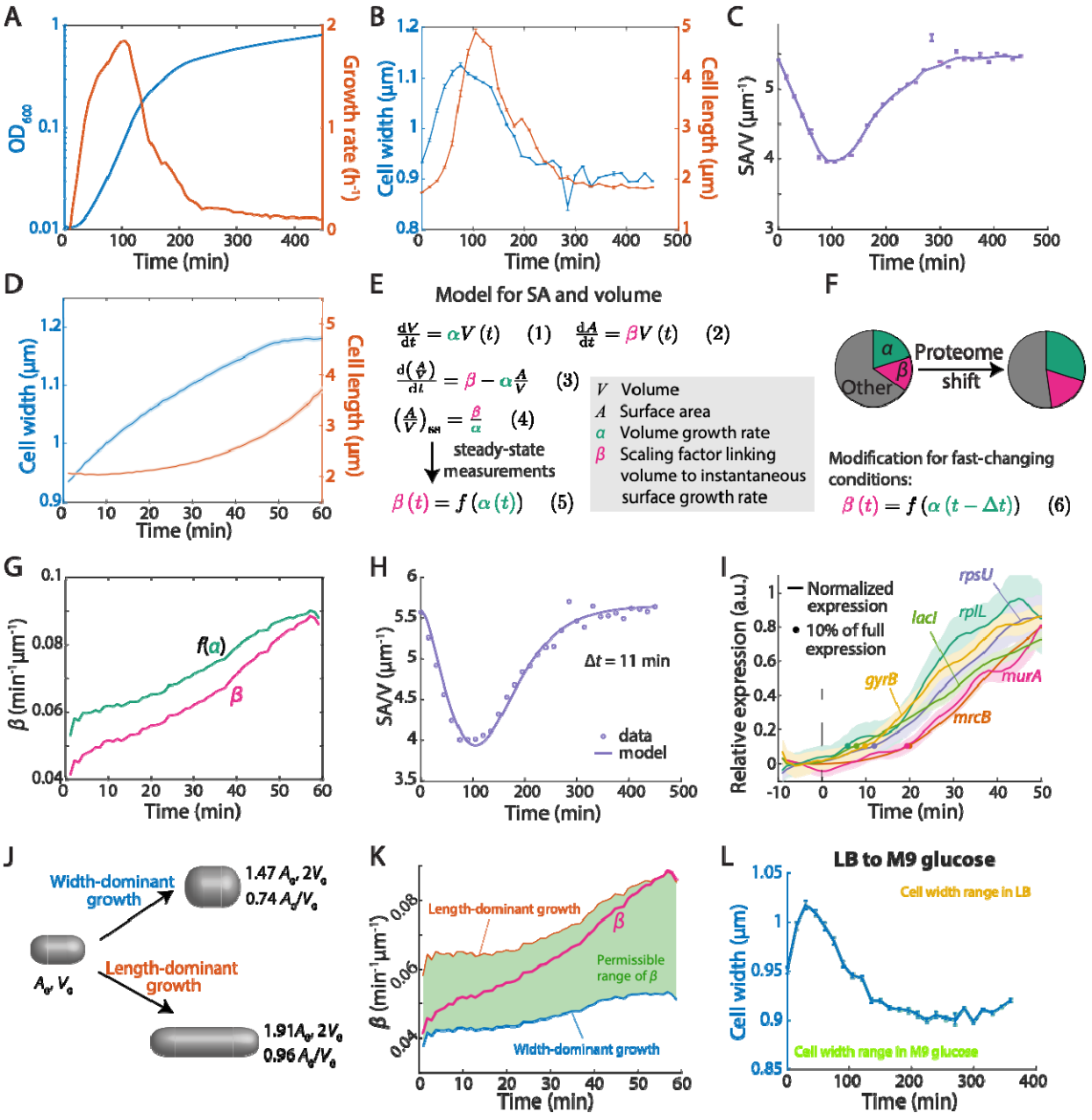

Figure 1: A time-delay model explains the relative dynamics of surface area and volume synthesis in batch cultures.

bioRxiv preprint doi: https://doi.org/10.1101/806885; this version posted October 17, 2019. The copyright holder for this preprint (which was not certified by peer review) is the author/funder. All rights reserved. No reuse allowed without permission.

673 A) Growth curve and the corresponding growth rate of an *E. coli* MG1655 batch
674 culture after diluting the overnight culture 1:200 into fresh LB. Growth rate peaks
675 at ~100 min post-dilution, and then slowly decreases.
676 B) Shape growth curves (cell width and length as a function of time) for the same
677 culture in (A). Cell width starts to increase earlier compared to length. Data
678 points are mean ± standard error of mean (s.e.m.) for $n > 200$ single cells.
679 C) SA/V as a function of time for the same culture in (B). SA/V decreased as cells
680 resume growth, and then slowly increased back to the initial value when cell
681 growth slowed down. Data points are mean ± s.e.m. with $n > 200$ single cells, and
682 the line is smoothed as a guide to the eye.
683 D) Single-cell time-lapse imaging of stationary-phase MG1655 cells diluted onto an
684 agarose pad containing fresh LB. Each cell exhibited similar width and length
685 dynamics as in the bulk culture in (B). Solid lines and the corresponding shaded
686 areas are mean ± s.e.m. with $n > 100$ single cells.
687 E) A conceptual model for SA/V regulation in cells. The synthesis rates of both
688 surface and volume scale with current cell volume (Eq. 1,2), predicting that the
689 time derivative of A/V depends on α, β, and the current A/V (Eq. 3). Steady state
690 A/V is therefore dictated by the ratio between β and α (Eq. 4). Using previous
691 experimental steady-state SA/V measurements, β can be parameterized as a
692 function of α in steady state (Eq. 5).

bioRxiv preprint doi: https://doi.org/10.1101/806885; this version posted October 17, 2019. The copyright holder for this preprint (which was not certified by peer review) is the author/funder. All rights reserved. No reuse allowed without permission.

F) Given that changes in growth rate (α) are accompanied by shifts in proteome composition, our model assumes that the shift is more heavily weighted toward cytoplasmic components than surface area components, thereby causing a delayed change in β, which can be approximated by introducing a constant time delay in the function relating β to α (Eq. 6).

G) From the single-cell data in (D), the experimentally measured β exhibited a delay of approximately 10 min compared to the steady-state β determined by Eq. 5 (i.e. $f(\alpha)$).

H) Fitting our time-delay model to the experimental data in (C) with $\Delta t = 11$ min yielded an excellent fit.

I) Protein expression levels were measured using GFP fused to the respective promoters and normalized from 0 to 1. The cytoplasmic proteins increased in expression ~10 min earlier than the cell-wall synthesis proteins. Dots represent the time points at which expression had increased by 10%. Data are mean ± standard deviation (S.D.) with $n > 100$ cells.

J) For a rod-shaped cell starting with surface area A_0 and V_0, doubling its volume by expansion in width costs 47% increase in surface area (top), whereas expansion in length requires a 91% increase in surface area (bottom). Therefore, an increase in width minimizes the surface area requirement for a given amount of volumetric growth.

bioRxiv preprint doi: https://doi.org/10.1101/806885; this version posted October 17, 2019. The copyright holder for this preprint (which was not certified by peer review) is the author/funder. All rights reserved. No reuse allowed without permission.

713 K) Given the geometry and instantaneous growth rate (α) of cells in (D), to maintain
714 rod-like shapes, only a certain range of β values are permissible (green;
715 Methods). The actual value of β started close to its minimal possible value,
716 characterizing a widening-dominant growth mode; by 60 min, β reached its
717 maximum possible value, transitioning to an elongation-dominant growth mode.
718 L) Dilution of stationary-phase cells grown in LB into M9 glucose caused increased
719 cell width, despite the fact that cells continuously passaged in M9 glucose always
720 had lower cell width than the LB-grown stationary-phase cells. Data are mean ±
721 s.e.m. with $n > 100$ cells.

bioRxiv preprint doi: https://doi.org/10.1101/806885; this version posted October 17, 2019. The copyright holder for this preprint (which was not certified by peer review) is the author/funder. All rights reserved. No reuse allowed without permission.

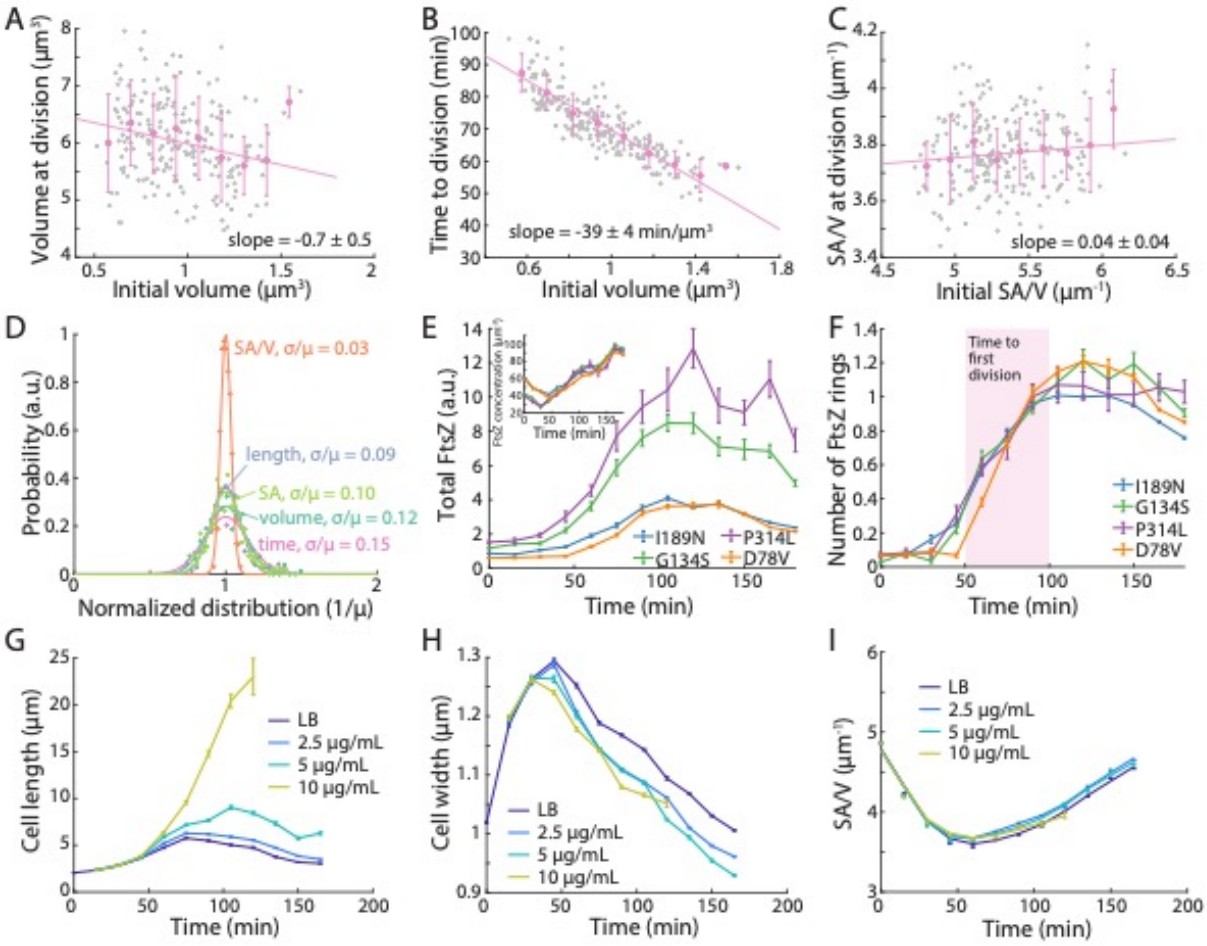

Figure 2: SA/V dynamics are correlated with cell division, and are conserved across cell morphologies.

A) For cells exiting stationary phase, the volume at the first division was negatively correlated with the starting volume, deviating from the "sizer" and "adder" models. Gray dots are data points for n = 209 individual cells, and pink data points are binned mean and S.D. values, which were fit to a linear model, leading to a slope of -0.7 ± 0.5 (mean ± s.e.m., Pearson's r = -0.22, p = 0.001, Student's t-test).

bioRxiv preprint doi: https://doi.org/10.1101/806885; this version posted October 17, 2019. The copyright holder for this preprint (which was not certified by peer review) is the author/funder. All rights reserved. No reuse allowed without permission.

B) The time to first division after stationary-phase exit was negatively correlated with the initial cell volume with a slope of -39 ± 4 min/μm^3 (mean ± s.e.m., Pearson's r = -0.86, $p < 10^{-5}$, Student's t-test), indicating that the first division was not regulated by time spent in fresh media. Gray dots are data points for n = 209 individual cells, and pink data points are binned mean and S.D. values.

C) The SA/V at the first division was largely constant and independent of the initial SA/V of the stationary-phase cell. Gray dots are data points for n = 209 individual cells, and pink data points are binned mean and S.D. values, which were fit to a linear model, leading to a slope of -0.04 ± 0.04 (mean ± s.e.m., Pearson's r = 0.11, p = 0.12, Student's t-test).

D) Normalized distributions of cell length, SA, volume, SA/V, and time at first division after stationary-phase exit. SA/V had by far the narrowest distribution, suggesting that the first cell division after exiting stationary phase occurs precisely at a fixed SA/V.

E) FtsZ abundance was measured as total fluorescence intensity inside cells. The dynamics of FtsZ regulation were similar across mutants. FtsZ abundance did not change in the first ~50 min, then increased to a maximum at ~100 min. Inset: While larger cells tended to have lower SA/V and higher FtsZ levels, FtsZ concentrations were highly similar across shape mutants. Data points are mean ± s.e.m. with n > 200 cells.

bioRxiv preprint doi: https://doi.org/10.1101/806885; this version posted October 17, 2019. The copyright holder for this preprint (which was not certified by peer review) is the author/funder. All rights reserved. No reuse allowed without permission.

F) All strains started without FtsZ rings and did not possess a ring until ~50 min post-dilution, consistent with the onset of first divisions after stationary phase exit (B). By 100 min, virtually all cells had ~1 FtsZ ring. Data points are mean ± s.e.m. with $n > 200$ cells.

G-I) Shape growth curves of *E. coli* MG1655 cells treated with sub-lethal concentrations of cephalexin. Cephalexin causes a dose-dependent increase in cell length (G), accompanied by decreased cell width (H). The increased lengths and decreased widths precisely maintain SA/V for all conditions (I), suggesting that SA/V is robust to perturbations in cellular dimensions. Data points are mean ± s.e.m. with $n > 200$ cells.

bioRxiv preprint doi: https://doi.org/10.1101/806885; this version posted October 17, 2019. The copyright holder for this preprint (which was not certified by peer review) is the author/funder. All rights reserved. No reuse allowed without permission.

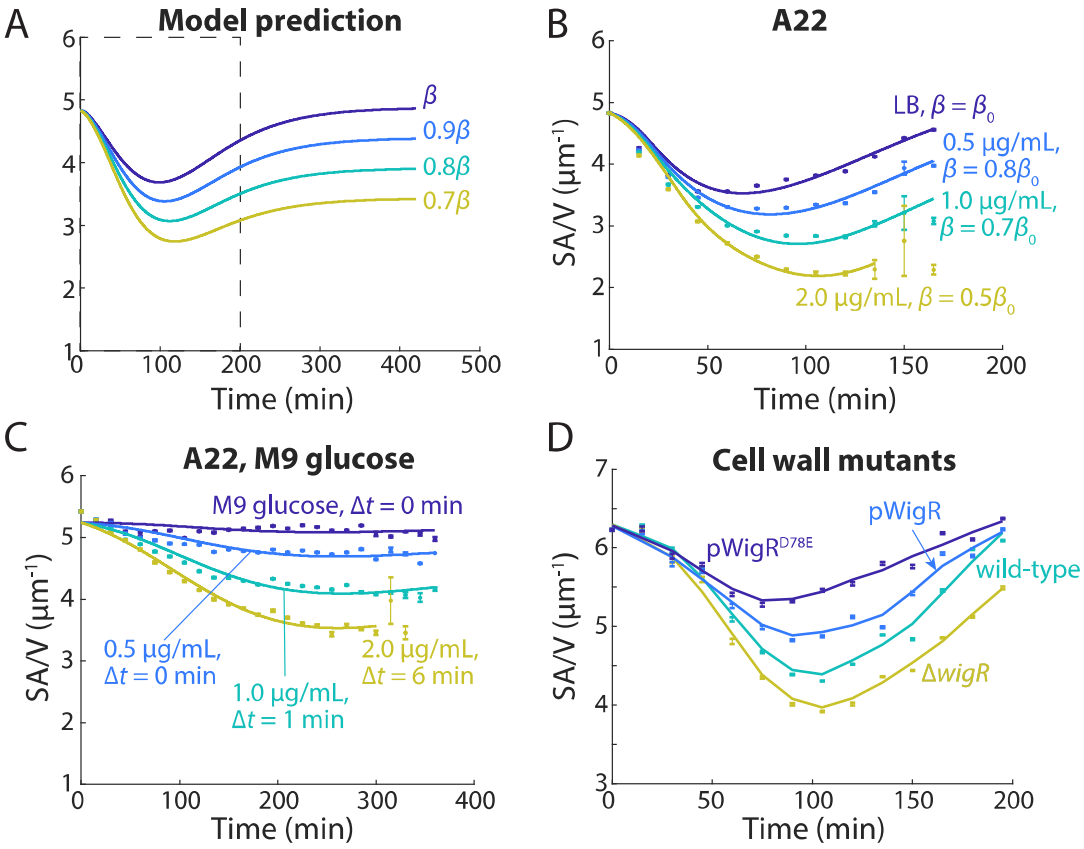

Figure 3: Time-delay model quantitatively predicts SA/V decreases due to inhibiting cell-wall synthesis.

A) The model predicts that decreasing β results in decreased SA/V over time.

B) Shape growth curves during A22 treatment in LB exhibited similar SA/V dynamics as predicted in (A).

C) Shape growth curves with A22 treatment in M9 glucose also exhibited decreases in SA/V, even though SA/V remained largely constant without A22. Higher A22 concentrations also led to non-zero Δt, indicating that cells must adjust their proteome under inhibition of cell-wall synthesis.

bioRxiv preprint doi: https://doi.org/10.1101/806885; this version posted October 17, 2019. The copyright holder for this preprint (which was not certified by peer review) is the author/funder. All rights reserved. No reuse allowed without permission.

771 D) Shape growth curves for *V. cholerae* cell-wall synthesis mutants. Overexpression
772 of WigR (pWigR, pWigR^{D78E}), which up-regulates cell wall synthesis without
773 affecting growth, increased SA/V. By contrast, Δ*wigR* cells have down-regulated
774 cell-wall synthesis and exhibited lower SA/V.

bioRxiv preprint doi: https://doi.org/10.1101/806885; this version posted October 17, 2019. The copyright holder for this preprint (which was not certified by peer review) is the author/funder. All rights reserved. No reuse allowed without permission.

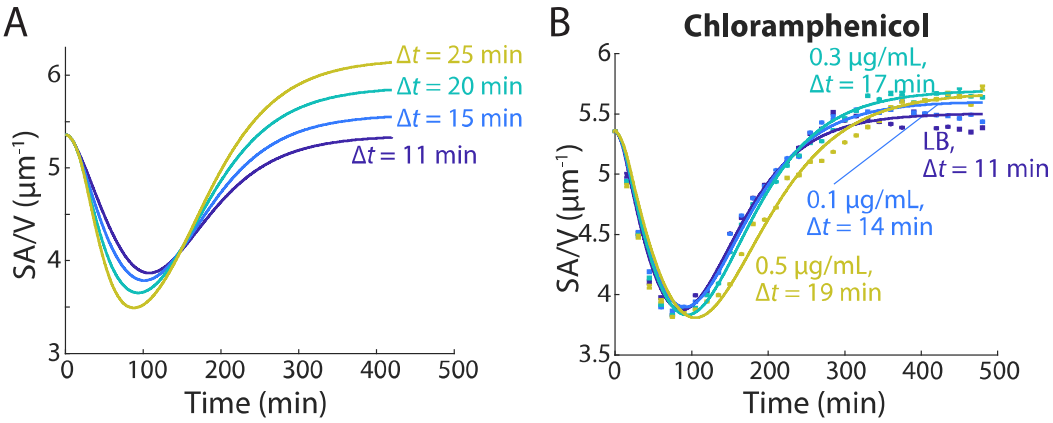

775

776 **Figure 4: Inhibiting translation increases the time delay between volume and surface**

777 **growth.**

778 A) The model predicts that higher Δt leads to lower SA/V in log phase, but higher

779 SA/V when cells enter stationary phase again.

780 B) Shape growth curves of MG1655 cells treated with low levels of

781 chloramphenicol. The dose-dependent SA/V dynamics were consistent with

782 model predictions, and model fitting resulted in longer Δt at higher doses. Data

783 points are mean ± s.e.m., with $n > 200$. Solid lines are best fits to the time-delay

784 model.

785

bioRxiv preprint doi: https://doi.org/10.1101/806885; this version posted October 17, 2019. The copyright holder for this preprint (which was not certified by peer review) is the author/funder. All rights reserved. No reuse allowed without permission.

Acknowledgements

The authors thank Alexandre Colavin, Linfeng Yang, Leigh Harris, Po-Yi Ho, and Petra Levin for helpful discussions, and Tobias Dörr and Suckjoon Jun for strains. This work was supported by NIH Director's New Innovator Awards DP2OD006466 (to K.C.H.), NSF CAREER Award MCB-1149328 (to K.C.H.), the Allen Center for Systems Modeling of Infection (to K.C.H.), and an Agilent Graduate Fellowship and a Stanford Interdisciplinary Graduate Fellowship (to H.S.). K.C.H. is a Chan Zuckerberg Biohub Investigator.

Data availability statement

The datasets generated during and/or analysed during the current study are available from the corresponding author on reasonable request.

bioRxiv preprint doi: https://doi.org/10.1101/806885; this version posted October 17, 2019. The copyright holder for this preprint (which was not certified by peer review) is the author/funder. All rights reserved. No reuse allowed without permission.

References

1 Magnusson, L. U., Farewell, A. & Nyström, T. ppGpp: a global regulator in Escherichia coli. *Trends in microbiology* **13**, 236-242 (2005).

2 Sutterlin, H. A. *et al.* Disruption of lipid homeostasis in the Gram-negative cell envelope activates a novel cell death pathway. *Proceedings of the National Academy of Sciences* **113**, E1565-E1574 (2016).

3 Siegele, D. A. & Kolter, R. Isolation and characterization of an Escherichia coli mutant defective in resuming growth after starvation. *Genes & development* **7**, 2629-2640 (1993).

4 Peters, J. M. *et al.* A comprehensive, CRISPR-based functional analysis of essential genes in bacteria. *Cell* **165**, 1493-1506 (2016).

5 Schaechter, M., Maaløe, O. & Kjeldgaard, N. O. Dependency on medium and temperature of cell size and chemical composition during balanced growth of Salmonella typhimurium. *Microbiology* **19**, 592-606 (1958).

6 Si, F. *et al.* Invariance of initiation mass and predictability of cell size in Escherichia coli. *Current Biology* **27**, 1278-1287 (2017).

7 Scott, M., Gunderson, C. W., Mateescu, E. M., Zhang, Z. & Hwa, T. Interdependence of cell growth and gene expression: origins and consequences. *Science* **330**, 1099-1102 (2010).

bioRxiv preprint doi: https://doi.org/10.1101/806885; this version posted October 17, 2019. The copyright holder for this preprint (which was not certified by peer review) is the author/funder. All rights reserved. No reuse allowed without permission.

8 Peebo, K. *et al.* Proteome reallocation in Escherichia coli with increasing specific growth rate. *Molecular BioSystems* **11**, 1184-1193 (2015).

9 Colavin, A., Shi, H. & Huang, K. C. RodZ modulates geometric localization of the bacterial actin MreB to regulate cell shape. *Nature communications* **9**, 1280 (2018).

10 Shi, H. *et al.* Deep phenotypic mapping of bacterial cytoskeletal mutants reveals physiological robustness to cell size. *Current Biology* **27**, 3419-3429. e3414 (2017).

11 Erickson, D. W. *et al.* A global resource allocation strategy governs growth transition kinetics of Escherichia coli. *Nature* **551**, 119 (2017).

12 Young, K. D. The selective value of bacterial shape. *Microbiol. Mol. Biol. Rev.* **70**, 660-703 (2006).

13 Typas, A., Banzhaf, M., Gross, C. A. & Vollmer, W. From the regulation of peptidoglycan synthesis to bacterial growth and morphology. *Nature Reviews Microbiology* **10**, 123 (2012).

14 Gitai, Z., Dye, N. & Shapiro, L. An actin-like gene can determine cell polarity in bacteria. *Proceedings of the National Academy of Sciences* **101**, 8643-8648 (2004).

15 Ursell, T. S. *et al.* Rod-like bacterial shape is maintained by feedback between cell curvature and cytoskeletal localization. *Proceedings of the National Academy of Sciences* **111**, E1025-E1034 (2014).

16 Bi, E. & Lutkenhaus, J. Cell division inhibitors SulA and MinCD prevent formation of the FtsZ ring. *Journal of bacteriology* **175**, 1118-1125 (1993).

bioRxiv preprint doi: https://doi.org/10.1101/806885; this version posted October 17, 2019. The copyright holder for this preprint (which was not certified by peer review) is the author/funder. All rights reserved. No reuse allowed without permission.

17 Harris, L. K., Dye, N. A. & Theriot, J. A. AC aulobacter MreB mutant with irregular cell shape exhibits compensatory widening to maintain a preferred surface area to volume ratio. *Molecular microbiology* **94**, 988-1005 (2014).

18 Zheng, H. *et al.* Interrogating the Escherichia coli cell cycle by cell dimension perturbations. *Proceedings of the National Academy of Sciences* **113**, 15000-15005 (2016).

19 Ursell, T. *et al.* Rapid, precise quantification of bacterial cellular dimensions across a genomic-scale knockout library. *BMC biology* **15**, 17 (2017).

20 Ouzounov, N. *et al.* MreB orientation correlates with cell diameter in Escherichia coli. *Biophysical journal* **111**, 1035-1043 (2016).

21 Monds, R. D. *et al.* Systematic perturbation of cytoskeletal function reveals a linear scaling relationship between cell geometry and fitness. *Cell reports* **9**, 1528-1537 (2014).

22 Harris, L. K. & Theriot, J. A. Relative rates of surface and volume synthesis set bacterial cell size. *Cell* **165**, 1479-1492 (2016).

23 Zaslaver, A. *et al.* A comprehensive library of fluorescent transcriptional reporters for Escherichia coli. *Nature methods* **3**, 623 (2006).

24 Pritchard, R. & Zaritsky, A. Effect of thymine concentration on the replication velocity of DNA in a thymineless mutant of Escherichia coli. *Nature* **226**, 126 (1970).

bioRxiv preprint doi: https://doi.org/10.1101/806885; this version posted October 17, 2019. The copyright holder for this preprint (which was not certified by peer review) is the author/funder. All rights reserved. No reuse allowed without permission.

25 Willis, L. & Huang, K. C. Sizing up the bacterial cell cycle. *Nature Reviews Microbiology* **15**, 606 (2017).

26 Moore, D. A., Whatley, Z. N., Joshi, C. P., Osawa, M. & Erickson, H. P. Probing for Binding Regions of the FtsZ Protein Surface through Site-Directed Insertions: Discovery of Fully Functional FtsZ-Fluorescent Proteins. *J Bacteriol* **199**, doi:10.1128/JB.00553-16 (2017).

27 Spratt, B. G. Distinct penicillin binding proteins involved in the division, elongation, and shape of Escherichia coli K12. *Proceedings of the National Academy of Sciences* **72**, 2999-3003 (1975).

28 Stouthamer, A. A theoretical study on the amount of ATP required for synthesis of microbial cell material. *Antonie van Leeuwenhoek* **39**, 545-565 (1973).

29 Iwai, N., Nagai, K. & Wachi, M. Novel S-benzylisothiourea compound that induces spherical cells in Escherichia coli probably by acting on a rod-shape-determining protein (s) other than penicillin-binding protein 2. *Bioscience, biotechnology, and biochemistry* **66**, 2658-2662 (2002).

30 Gitai, Z., Dye, N. A., Reisenauer, A., Wachi, M. & Shapiro, L. MreB actin-mediated segregation of a specific region of a bacterial chromosome. *Cell* **120**, 329-341 (2005).

bioRxiv preprint doi: https://doi.org/10.1101/806885; this version posted October 17, 2019. The copyright holder for this preprint (which was not certified by peer review) is the author/funder. All rights reserved. No reuse allowed without permission.

31 Kahan, F. M., Kahan, J. S., Cassidy, P. J. & Kropp, H. The mechanism of action of fosfomycin (phosphonomycin). *Annals of the New York Academy of Sciences* **235**, 364-386 (1974).

32 Marquardt, J. L. *et al.* Kinetics, stoichiometry, and identification of the reactive thiolate in the inactivation of UDP-GlcNAc enolpyruvoyl transferase by the antibiotic fosfomycin. *Biochemistry* **33**, 10646-10651 (1994).

33 Banzhaf, M. *et al.* Cooperativity of peptidoglycan synthases active in bacterial cell elongation. *Molecular microbiology* **85**, 179-194 (2012).

34 Dörr, T. *et al.* A cell wall damage response mediated by a sensor kinase/response regulator pair enables beta-lactam tolerance. *Proceedings of the National Academy of Sciences* **113**, 404-409 (2016).

35 Vadia, S. *et al.* Fatty acid availability sets cell envelope capacity and dictates microbial cell size. *Current Biology* **27**, 1757-1767. e1755 (2017).

36 Klieneberger, E. The natural occurrence of pleuropneumonia-like organism in apparent symbiosis with Strrptobacillus moniliformis and other bacteria. *The Journal of Pathology and Bacteriology* **40**, 93-105 (1935).

37 Schmidt, A. *et al.* The quantitative and condition-dependent Escherichia coli proteome. *Nature biotechnology* **34**, 104 (2016).

38 Levy, D. L. & Heald, R. Mechanisms of intracellular scaling. *Annual review of cell and developmental biology* **28**, 113-135 (2012).

bioRxiv preprint doi: https://doi.org/10.1101/806885; this version posted October 17, 2019. The copyright holder for this preprint (which was not certified by peer review) is the author/funder. All rights reserved. No reuse allowed without permission.

39 van Helvoort, J. M. & Woldringh, C. L. Nucleoid partitioning in Escherichia coli during steady-state growth and upon recovery from chloramphenicol treatment. *Molecular microbiology* **13**, 577-583 (1994).

40 Ho, P.-Y. & Amir, A. Simultaneous regulation of cell size and chromosome replication in bacteria. *Frontiers in microbiology* **6**, 662 (2015).

41 Taheri-Araghi, S. *et al.* Cell-size control and homeostasis in bacteria. *Current Biology* **25**, 385-391 (2015).

42 Si, F. *et al.* Mechanistic origin of cell-size control and homeostasis in bacteria. *Current Biology* **29**, 1760-1770. e1767 (2019).

43 Sekar, K. *et al.* Synthesis and degradation of FtsZ quantitatively predict the first cell division in starved bacteria. *Molecular systems biology* **14** (2018).

44 Brownlee, C. & Heald, R. Importin α partitioning to the plasma membrane regulates intracellular scaling. *Cell* **176**, 805-815. e808 (2019).

45 Billings, G. *et al.* De novo morphogenesis in L-forms via geometric control of cell growth. *Molecular microbiology* **93**, 883-896 (2014).

46 Stuurman, N., Amdodaj, N. & Vale, R. μManager: open source software for light microscope imaging. *Microscopy Today* **15**, 42-43 (2007).

bioRxiv preprint doi: https://doi.org/10.1101/806885; this version posted October 17, 2019. The copyright holder for this preprint (which was not certified by peer review) is the author/funder. All rights reserved. No reuse allowed without permission.

914 47 Sliusarenko, O., Heinritz, J., Emonet, T. & Jacobs-Wagner, C. High-throughput,
915 subpixel precision analysis of bacterial morphogenesis and intracellular spatio-
916 temporal dynamics. *Molecular microbiology* **80**, 612-627 (2011).
917

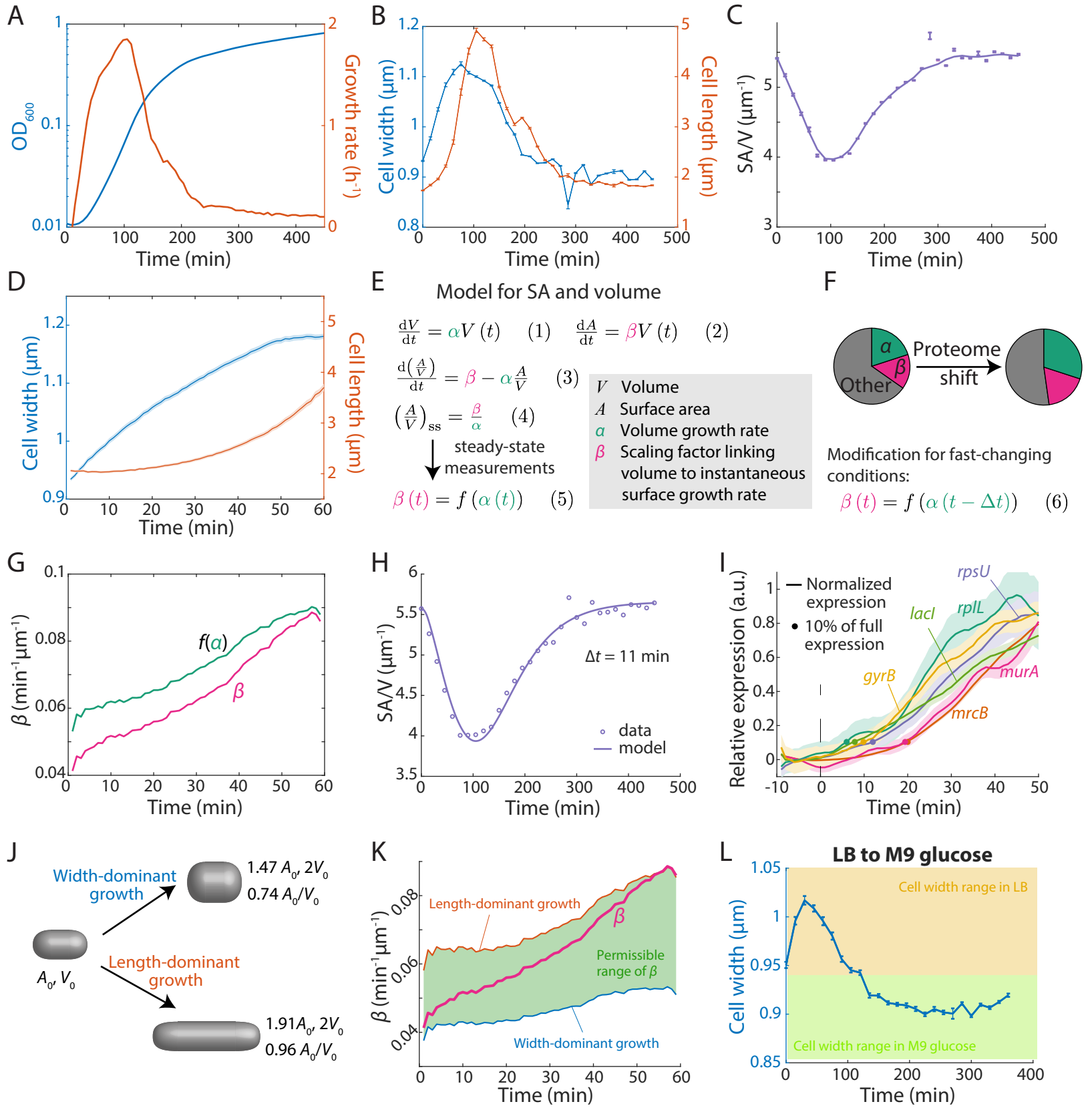
A
OD600
Growth rate (h-1)
Time (min)
B
Cell width (μm)
Cell length (μm)
Time (min)
C
SA/V (μm-1)
Time (min)
D
Cell width (μm)
Cell length (μm)
Time (min)
E
Model for SA and volume
dV/dt = αV(t) (1)
dA/dt = βV(t) (2)
d(A/V)/dt = β − α A/V (3)
(A/V)ss = β/α (4)
steady-state measurements
β(t) = f(α(t)) (5)
V Volume
A Surface area
α Volume growth rate
β Scaling factor linking volume to instantaneous surface growth rate
F
α
β
Other
Proteome shift
Modification for fast-changing conditions:
β(t) = f(α(t − Δt)) (6)
G
β (min-1 μm-1)
f(α)
β
Time (min)
H
SA/V (μm-1)
Δt = 11 min
data
model
Time (min)
I
Relative expression (a.u.)
Normalized expression
10% of full expression
rpsU
rplL
lacI
gyrB
murA
mrcB
Time (min)
J
Width-dominant growth
1.47 A0, 2V0
0.74 A0/V0
A0, V0
Length-dominant growth
1.91A0, 2V0
0.96 A0/V0
K
Length-dominant growth
β
Permissible range of β
Width-dominant growth
β (min-1 μm-1)
Time (min)
L
LB to M9 glucose
Cell width range in LB
Cell width range in M9 glucose
Cell width (μm)
Time (min)

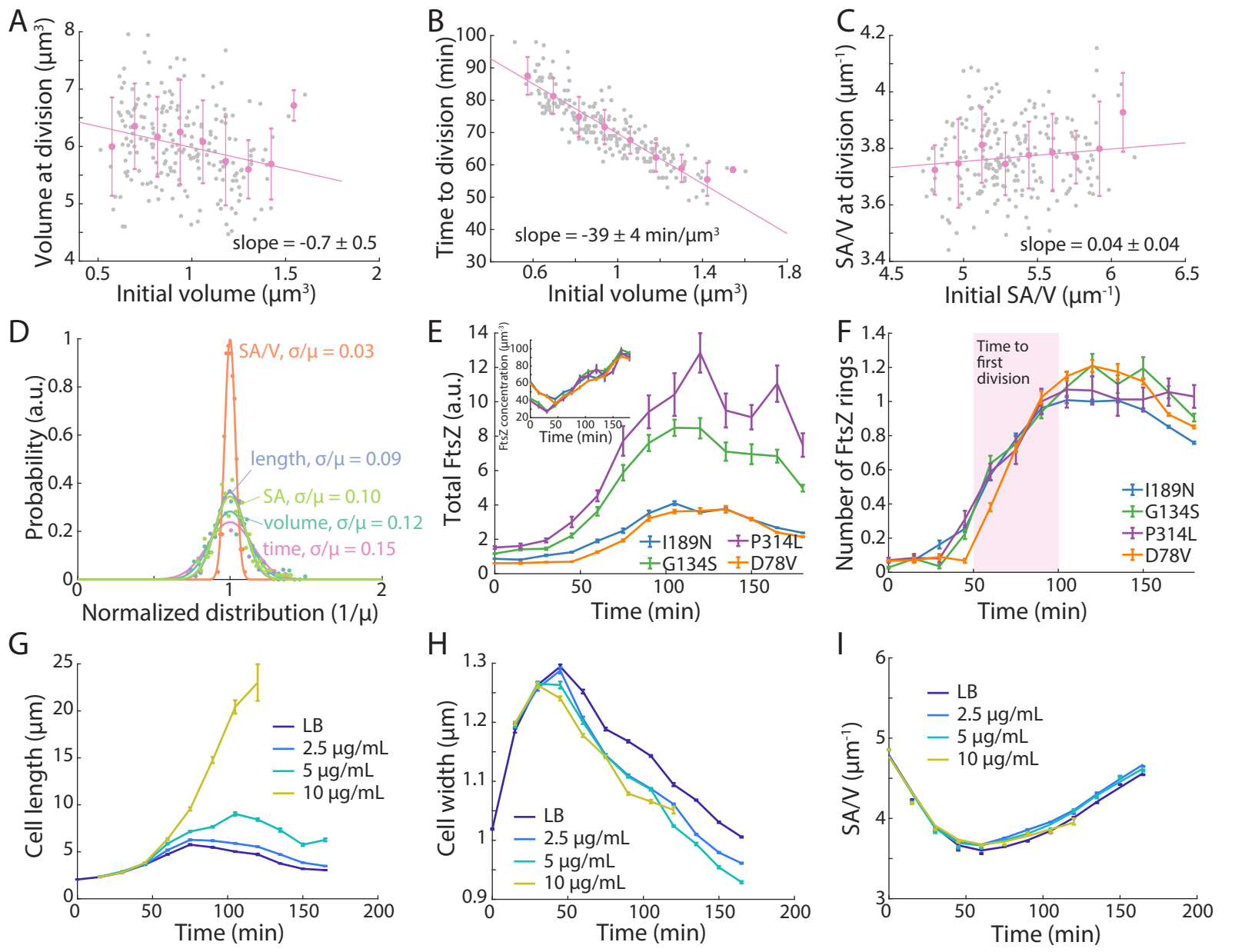
A
Volume at division (μm³)
Initial volume (μm³)
slope = -0.7 ± 0.5
B
Time to division (min)
Initial volume (μm³)
slope = -39 ± 4 min/μm³
C
SA/V at division (μm⁻¹)
Initial SA/V (μm⁻¹)
slope = 0.04 ± 0.04
D
Probability (a.u.)
Normalized distribution (1/μ)
SA/V, σ/μ = 0.03
length, σ/μ = 0.09
SA, σ/μ = 0.10
volume, σ/μ = 0.12
time, σ/μ = 0.15
E
Total FtsZ (a.u.)
Time (min)
FtsZ concentration (μm⁻³)
I189N
P314L
G134S
D78V
F
Number of FtsZ rings
Time (min)
Time to first division
I189N
G134S
P314L
D78V
G
Cell length (μm)
Time (min)
LB
2.5 μg/mL
5 μg/mL
10 μg/mL
H
Cell width (μm)
Time (min)
LB
2.5 μg/mL
5 μg/mL
10 μg/mL
I
SA/V (μm⁻¹)
Time (min)
LB
2.5 μg/mL
5 μg/mL
10 μg/mL

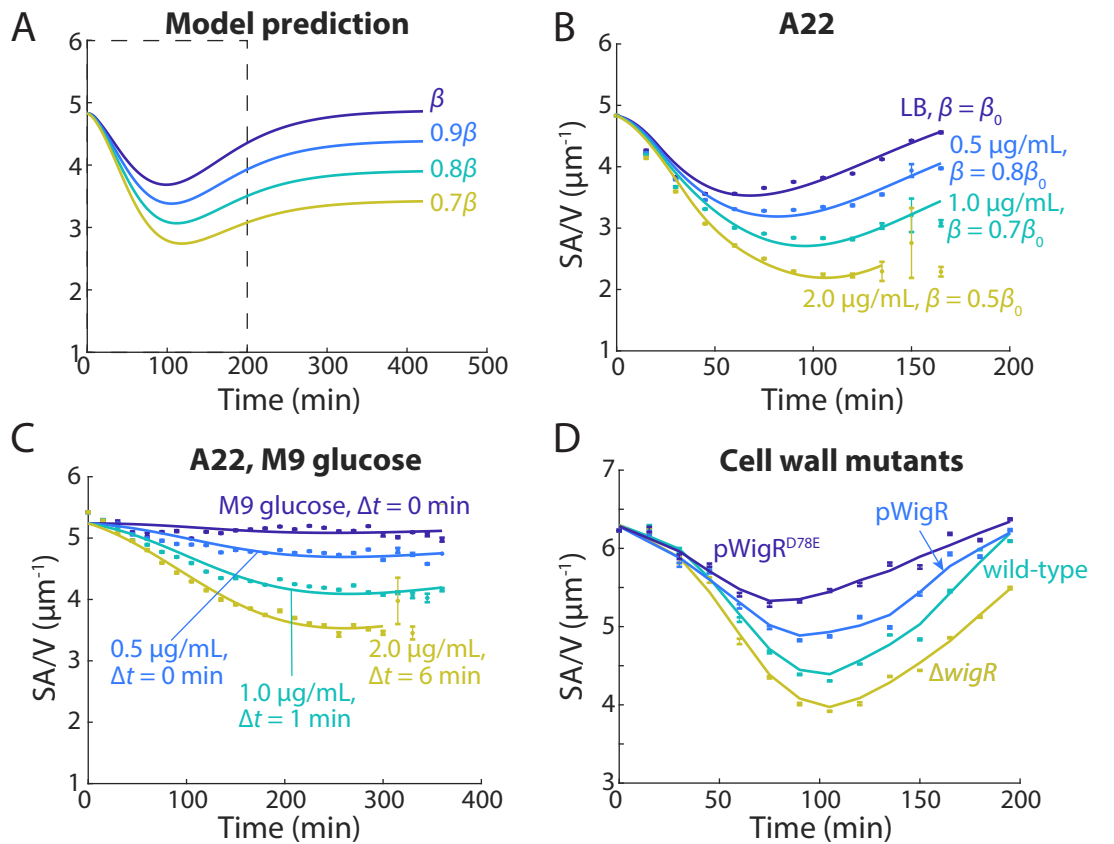
A
Model prediction
β
0.9β
0.8β
0.7β
Time (min)
B
A22
LB, β = β0
0.5 μg/mL, β = 0.8β0
1.0 μg/mL, β = 0.7β0
2.0 μg/mL, β = 0.5β0
SA/V (μm-1)
Time (min)
C
A22, M9 glucose
M9 glucose, Δt = 0 min
0.5 μg/mL, Δt = 0 min
1.0 μg/mL, Δt = 1 min
2.0 μg/mL, Δt = 6 min
SA/V (μm-1)
Time (min)
D
Cell wall mutants
pWigR
pWigRD78E
wild-type
ΔwigR
SA/V (μm-1)
Time (min)

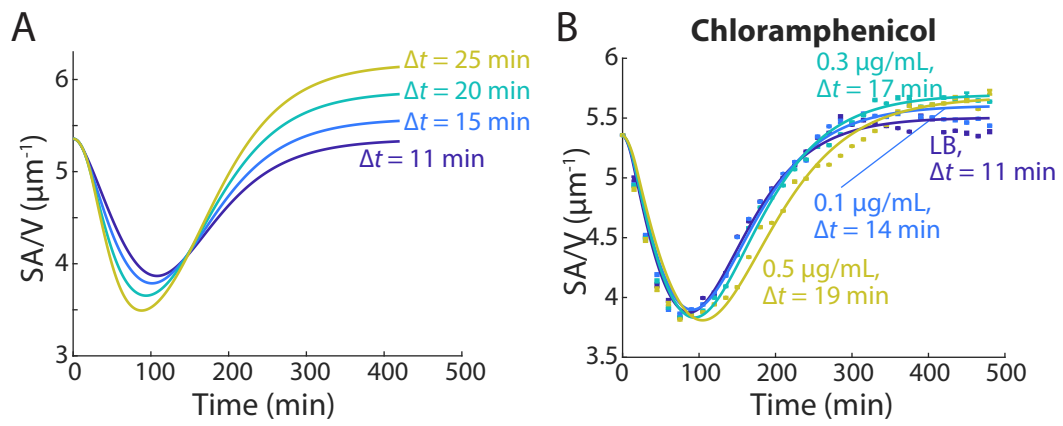
A
Δt = 25 min
Δt = 20 min
Δt = 15 min
Δt = 11 min
SA/V (μm-1)
Time (min)
B
Chloramphenicol
0.3 μg/mL,
Δt = 17 min
LB,
Δt = 11 min
0.1 μg/mL,
Δt = 14 min
0.5 μg/mL,
Δt = 19 min
SA/V (μm-1)
Time (min)